⊙ 論 文

A Numerical Simulation of a Viscous Flow behind a Sea-bottom Isolated Ridge in Shallow Water

by Young-Gill Lee*, Hideaki Miyata**, Guen Moo Lee***

(1992년 1월 28일 접수)

천해수역에 위치한 3차원 해저돌출물 주위 점성유동장의 수치시뮬레이션

이 영 길* · Hideaki Miyata** · 이 무 근***

Key Words : Finite-Difference Method(有限差分法), Rectangular Coordinate System (직사각형 格子系), Shallow Water(淺水), Projecting Part of Sea-bottom (海底突出物), Free-Surface(自由表面), Viscous Flow Field(粘性 流動場), Interaction of Eddies(渦動의 상호간섭), Plane-Porosity(面 포로시티), Volume-Porosity(體積 포로시티)

초 록

自由表面下에 잠긴 복잡한 三次元 物體 周圍의 흐름을 解析하기 위한 數値 計算法이 TUMMAC(Tokyo Univ. Modified Marker And Cell)法을 基礎로 하여 開發되었다. 임의 物體의 no-slip 三次元 物體表面條件을 보다 간단히 처리하기 위하여 "porosity"라는 개념이 도입되었으며, 淺水域에 잠겨 있는 海底突出物 周圍의 流動을 計算하여 그 應用性을 검토하였다. 突出物 後方의 복잡한 渦動들의 상호간섭이 잘 시뮬레이션 되었다.

1. Introduction

The analysis of the flow and wave-making phenomena around a physical solid is an important subject in the fields of naval architecture, ocean and coastal engineering. Especially, the analysis of fluid dynamic characteristics for the currents and waves which is influenced with the topography of ocean is one of the most important research filed. The flows around the bodies of offshore structure or the projecting parts of sea-bottom accompanies complicated vortical motions. Moreover, these become more complicated phenomena in the vicinity of a free-surface. For a long time,

* Member, Powering Performance Lab., Korea Research Institute of Ships and Ocean Engineering
** Department of Naval Architecture and Ocean Engineering, The University of Tokyo, JAPAN
*** Department of Naval Architecture, Hongik Technical College

potential and boundary layer theories have been used to analyze the general features of the flow pattern around a smooth hull surface or a simplified surface of an offshore structure. However, the flows after separation and the nonlinear free-surface have been very roughly treated, because these have very complicated features and the classical theories could not deal with these problems. Therefore, the nonlinear phenomena of wave breaking, vortex generation, flow separation and so forth which take place on the complex offshore structure piercing the free-surface have been mostly treated with experimental methods.

Yamada and Miyata[1] suggested the TUMMAC-Ⅶ method using a fixed rectangular coordinate system that is applicable to simulate the viscous flow around a three-dimensional complicated body. They treated approximately no-slip body surface condition on the body boundary cells making use of two kinds of porosity parameters and demonstrated by the simulation of a viscous flow past a sphere at the Reynolds number 1000. The complete three-dimensional vortex shedding motion was qualitatively well simulated. Most of the numerical computation methods employ a body boundary fitted coordinate system. However, it will be impossible to generate a useful curvilinear grid system for the boundary surface of complex shape such as an offshore structure piercing the free-surface which is accompanied with violent nonlinear waves. In case of two-dimensional body, the authors had presented a finite-difference method(TUMMAC-V_{WV} method)[2,3] using an irregular leg length in order to treat the no-slip body boundary condition in the framework of a rectangular grid system. But, it may be difficult in three-dimensional case, because the program code is extremely complicated and the computation time is remarkably increased. Therefore, in order to simplify the treatment of the three-dimensional body boundary condition in a rectangular coordinate system, the idea or porosity is introduced in this paper. Moreover, the treatment technique of the free-surface conditions, which is used in the TUMMAC－Ⅳ method[4], is engaged for the computation of free-surface.

In order to investigate the applicability of present method, the newly-developed computational procedure is applied to the flow around a projecting part of sea-bottom in shallow water. For the research of this sort, we can cite a good number of papers across the world. Houghton and kasahara[5] investigate the nature of the hydraulic jumps in the flows across a two-dimensional ridge. They used the one-dimensional time-dependent "shallow water" equations for the motion of an incompressible, homogeneous, inviscid and hydrostatic fluid. The nonlinear phenomenon of the jumps was determined by using asymptotic solutions to the model equations. Lamb and Britter[6] performed the series of numerical and laboratory experiments for the flow over a three-dimensional obstacle in shallow water condition. They employed a finite-difference model in the numerical simulation of a homogeneous non-rotating flow. The results demonstrated how the flow over a three-dimensional obstacle deviates from the patterns established for a two-dimensional ridge. Miyata, Matsukawa and Kajitani[7] investigated the two-dimensional shallow water flow over an isolated obstacle by a numerical technique based on a finite-difference method (TUMMAC-V method). The computed results indicated that the viscous and free-surface flow in a shallow water condition cannot be explained without the understanding of wave breaking nature. Recently, a model for describing the discontinuous atmospheric flows over a monutain ridge was suggested by Cullen[8]. An

implicit finite-difference method using Lagrangian evolution equations was presented for modelling such flows.

The numerical computation method is elaborated in Section 2. the numerical simulation for a projecting part of sea-bottom and brief concluding remarks are given in Sections 3 and 4, respectively.

2. Numerical computation method

2. 1 Governing equations

The governing equations are the Navier-Stokes (N−S) equations and the continuity equation in the case of a three-dimensional incompressible fluid, and represented as follows.

$$\frac{\partial u_i}{\partial t} = -\frac{\partial \phi}{\partial x_i} - \frac{\partial \phi_t}{\partial x_i} - u_j\frac{\partial u_i}{\partial x_j} + \nu\frac{\partial}{\partial x_j}\cdot\left(\frac{\partial u_i}{\partial x_j}\right) + \nu_s\frac{\partial}{\partial x_j}\left(\frac{\partial u_i}{\partial x_j}\right) + \frac{\partial \nu_s}{\partial x_j}\left(\frac{\partial u_i}{\partial x_j} + \frac{\partial u_j}{\partial x_i}\right) + M_i + f_i, \quad \cdots\cdots (1)$$

$$\frac{\partial u_j}{\partial x_j} = 0, \quad \cdots\cdots (2)$$

where u is the velocity component in each direction, $\phi = p/r$(P ; pressure, ρ ; density), ϕ_t is turbulent pressure per unit density, ν is the kinematic viscosity and ν_s is the eddy viscosity coefficient from the SGS(Sub-Grid Scale) turbulence model. Also, M_i is the arbitrary numerical diffusion, dispersion or dissipation term for the stability of solution, and f_i is the external force per unit mass that is the gravitational acceleration in the case of vertical direction component.

2. 2 Grid system

The computational domain is discretized into a rectangular staggered mesh system. The staggered mesh system increase the computational accuracy of mass and momentum conservation property in comparison to a regular mesh system. Since the grid lines do not coincide with the body boundary and the free-surface, it can not be anticipated that the computational accuracy is good for the treatment of the body boundary and free-surface conditions. Also, the resolution of the flow simulation is not so high in the vicinity of the boundaries. However, an advantage of this grid system is that the required effort for the grid generation is negligibly small, which is most important for the practical applications.

In order to increase the computational accuracy, the body boundary and the free-surface conditions are implemented by several ingenious numerical techniques. That is, a generalized 2nd-order differential scheme and velocity-pressure simultaneous iterative method are used for the body boundary condition, an irregular star and the iterative calculation of marker point are used for the free-surface condition, respectively. Moreover, the computational domain is divided into two regions to increase of the computational efficiency. The two regions are the fluid region composed of fluid cells (F-cells) and the body boundary region composed of body boundary cells (B-cells). The details of the grid system are explained in reference(1) and (9).

2. 3 Boundary conditions

All cells used in the computational domain are classified into full-of-fluid cells (F-cells), body boundary cells(B-cells) and empty cells(E-cells). The configuration of a three-dimensional body is represented by two kinds of porosity in B-cells, that is, volume-porosity γ and plane-porosity β as shown in Fig. 1. The volume-porosity is the ratio of fluid portion in each cell and it is defined at a pressure point. The plane-porosity is the ratio

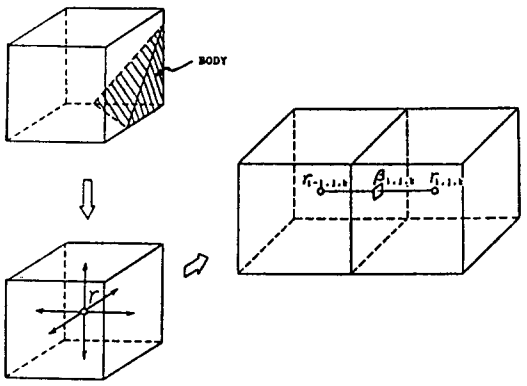

Fig. 1 Definition sketch of volume and plane porosity.

of fluid portion on each plane of a cell as expressed by equation (3) and it is defined at a velocity point.

$$\beta_{i+\frac{1}{2}} = (\gamma_i + \gamma_{i+1})/2. \quad \cdots\cdots\cdots\cdots\cdots\cdots \quad (3)$$

Moreover, the B-cell is flagged as a cell of which volume-porosity is greater than 0.5 but less than 1.0. A cell of which volume-porosity if less than 0.5 is flagged as E-cell. Also, a F-cell facing a E-cell is defined as a special B-cell(B*-cell in Fig. 2), because this cell can not be neighboured with six pressure points. Velocity point is

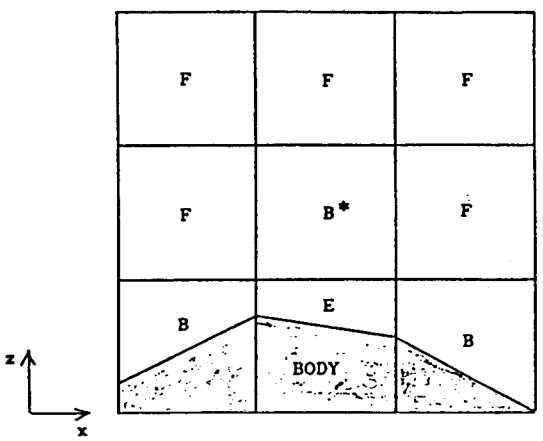

Fig. 2 Cell flagging in TUMMAC-Ⅶ sheme.

assumed to exist when the plane-porosity is greater than 0.5. Since the porosity is a scalar, it is used not only for the flagging of cells and for the calculation of flux and divergence but also for the choice of differencing scheme and for the calculation of first and second derivative terms in the governing equations.

For the no-slip body boundary condition, the velocity in a B-cell, of which plane-porosity is greater than 0.5 but less than 1.0, is interpolated by the neighbouring velocities and using the definition of zero-velocity at the body surface as shown in Fig. 3. The velocities, which are not

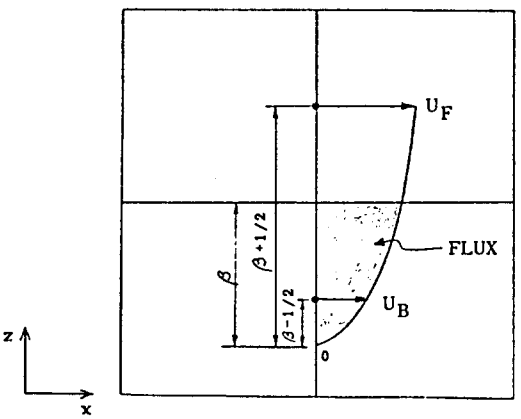

Fig. 3 Interpolation of velocity and definition of flux at a body boundary cell in TUMMAC-Ⅶ scheme.

interpolated themselves, are used for the interpolation of B-cell's velocities. Also, the plane-porosity of a cell, where neighbouring velocities are situated, is used as a weighting factor in the interpolation of a velocity using a quadratic equation. The no-slip condition is incorporated in the differencing scheme, too. In the vicinity of body surface, the modified second-order centered differencing is used for the convection and diffusion term considering the plane-porosity and zero-velocity on the body surface.

For the calculation of pressure in B-cells the following simultaneous iterative method is used, in order to suitably implement the zero-divergence condition in B-cells.

$$\phi^{m+1} = \phi^{m} + \frac{\omega}{AA} \cdot D, \quad \cdots\cdots (4)$$

$$AA = \triangle t \cdot \{ \frac{\gamma_{i+1}+\gamma_{i-1}}{(\triangle x)^2} + \frac{\gamma_{j+1}+\gamma_{j-1}}{(\triangle y)^2} + \frac{\gamma_{k+1}+\gamma_{k-1}}{(\triangle z)^2} \}, \quad \cdots\cdots (5)$$

where D is the divergence of a cell, m is the iteration number and ω is the relaxation factor.

In free-surface calculation, the exactly same technique with the TUMMAC－Ⅳ method[4] is employed. Namely, the Lagrangian movement of marker particles is used for the fulfilment of Chan and Street[10] is applied to the dynamic condition on that surface. Some interpolation and extrapolation techniques are employed for the determination of the velocity components at the position of a marker particle, i.e., four-point and nine-point interpolations and zero-gradient extrapolations are used.

At the inflow boundary both velocity and pressure distribution are set as the pre-determined values for a uniform flow. In the case of other boundaries the velocities and pressures are set equal to the inner values so that their gradients in the direction normal to the boundary are set zero, that is, a Neumann condition is employed.

2.4 Computational procedure

The computational algorithm of the TUMMAC－Ⅶ method are well explained in Yamada and Miyata(1), and very brief explanations are described here. The governing equations (1) and (2) are represented in finite-difference forms, and solved as an initial-and boundary-value problems including the free-surface conditions and using time-marching procedure and iteration methods. The N－S equations are represented by first-order forward diferencing in time and second-order centered differencing in a Cartesian coordinate system except for the convection terms. The differencing of the convection terms are described by a third-order upwind differencing scheme. The computation is started at a rested state, and the velocities in computational domain are gradually accelerated for a desired inflow velocity. After the steps of acceleration the computation is continued for an adequate time step, which is supposed to be a sufficient time to have almost steady state.

The momentum equations and continuity equation result in the Poisson equation for the pressure distribution. Updating of the velocity field is made after updating the pressure field by solving the Poisson equation and this cycle is repeated in the time-marching procedure. The velocity field is updated as the following equation.

$$u_i^{n+1} = u_i^{n} + \triangle t \left(- \frac{\partial \phi}{\partial x_i} - \frac{\partial \phi_t}{\partial x_i} - C_i + D_i + E_i + M_i + f_i \right)^n, \quad \cdots\cdots (6)$$

where n is the number of time step, C_i is the convection term, D_i is the diffusion term and E_i is the eddy viscous term. For the determination of the ϕ_t and E_i term, the SGS turbulence model[11] is incorporated into the present method so that a complicated flow in high Reynolds number may be presumably well simulated.

For the solution of the Poisson equation the following iteration formula is used in F-cells.

$$\phi_{i,j,k}^{m+1} = \phi_{i,j,k}^{m} + \omega(\phi_{i,j,k\,cal}^{m+1} - \phi_{i,j,k}^{m}), \quad \cdots (7)$$

where $\phi_{i,j,k}^{m+1}cal.$ is a temporary pressure at each iteration step. In order to maintain the stability of computation, the temporary pressure is explicitly determined in the all computational

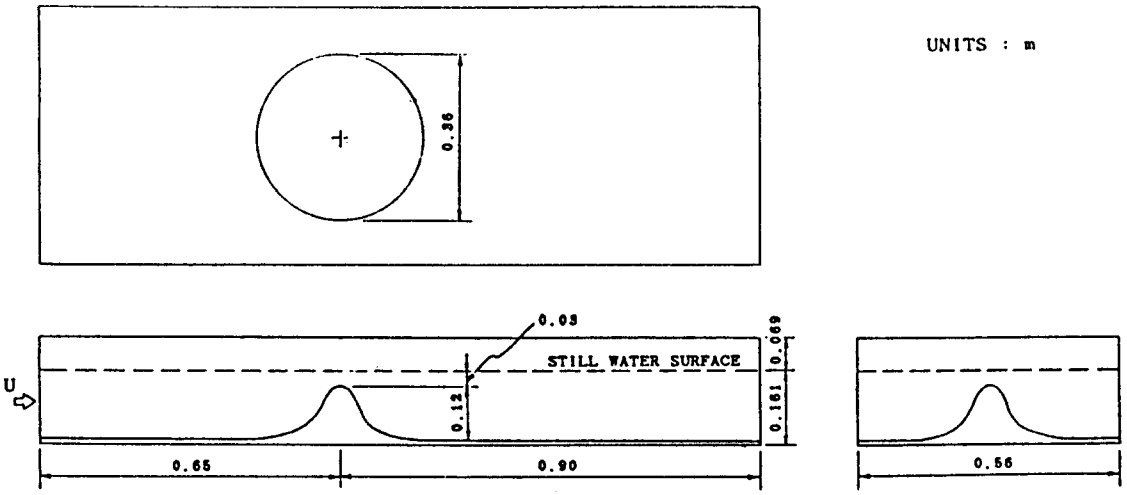

Fig. 4 Comptational domain for a isolated ridge in shallow water condition.

domain. The iteration is continued until the second term of Eq.(7) converges within an allowable error.

3. Numerical simulation

The applicability of the newly-developed numerical simulation method is examined by simulating the flow pattern around a projecting part of sea-bottom in shallow water condition. As shown in Fig. 4 the computation was performed about a three-dimensional projecting model of cone type with bottom diameter 0.36. The uniform flow which has a main velocity U=0.2m/s and an empirically determined velocity profile near the bottom surface are provided on inlet surface. Therefore, the Froude number based on the water depth is 0.165 and the Reynolds number based on the height of the projecting part is 23, 230. Any other non-dimensional value is based on the height of the projecting part in this paper. As clarified by Lamb and Britter[6], a hydraulic jump on the free-surface will not be appeared in this condition.

The grid system in the vicinity of projecting part is shown in Fig. 5. Since a cell size is uniformly 1cm×1cm×1cm all over the computational domain, the height of the projecting part is divided into 12 cells and the total number of cells is 139,000.

The computation is started from the rest condition, and the fluid all over the computational domain is accelerated for 1,000 time steps. After the acceleration is finished, the computation is conitnued to 3,000 time step (T=25.0, where T is the non-dimensional time).

The simulated results are shown in Figs. 6 to 12. The time-sequential development of the contour maps of vorticity is shown in Fig. 6, 7 and 8 for the cases of the Y−Z, X−Z and X−Y plane, respectively. The strength of vorticity is calculated by integrating the two-dimensional circulation of a cell and dividing it by the area of the each side surface in a cell. In these figures, O_1 is the vorticity of the x-axis vortex and O_2, O_3 are those of the y-and z-axis vortex, respectively. The contour pattern of O_1 is periodically repeated as observed in Fig. 6 and a large pair of vortices will be recurrently developed as shown at T=18. 7 in this figure. As shown in Fig. 7, shear flows

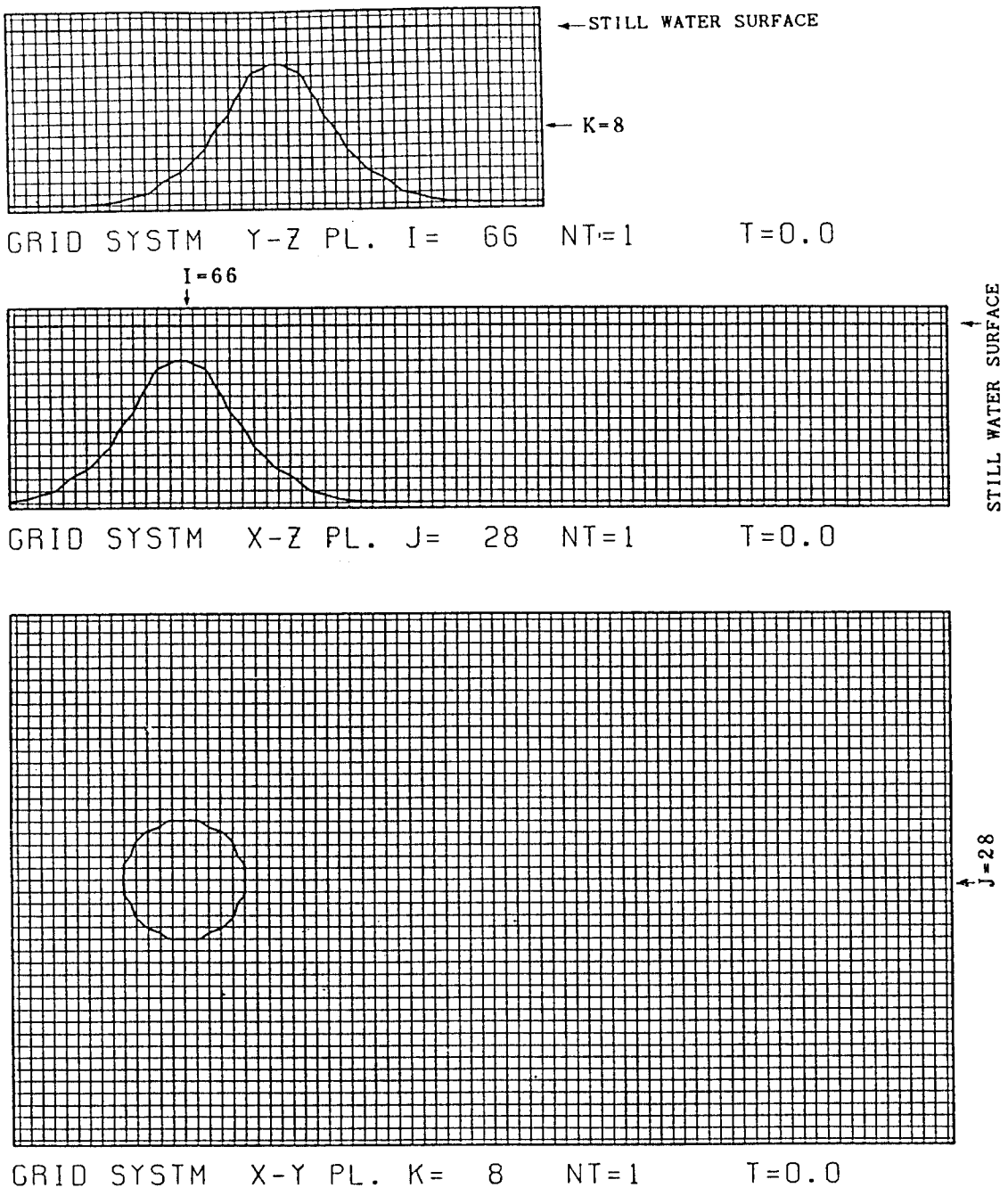

Fig. 5 Grid system in the vicinity of a isolated ridge in shallow water condition.

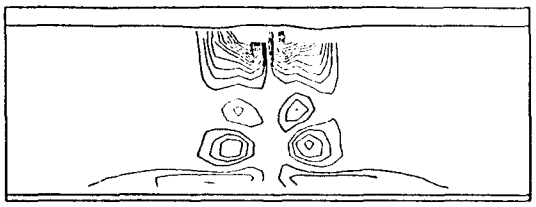

02 Contour X-Z PL. J=28 NT=2000 T=16.7

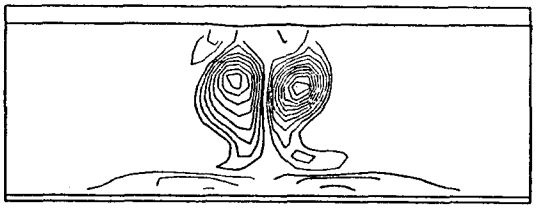

02 Contour X-Z PL. J=28 NT=2250 T=18.7

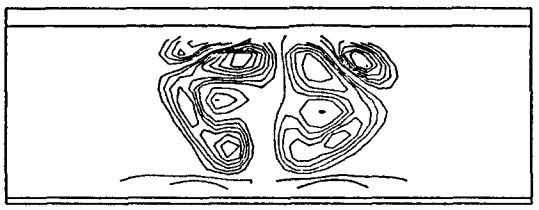

02 Contour X-Z PL. J=28 NT=2500 T=20.8

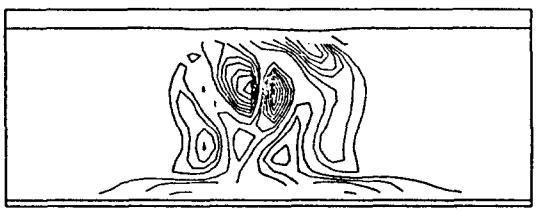

02 Contour X-Z PL. J=28 NT=2750 T=22.9

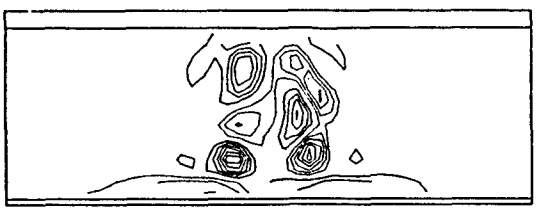

02 Contour X-Z PL. J=28 NT=3000 T=25.0

Fig. 6 Vorticity contour maps on the Y-Z plane I=102. Anticlockwise vorticity is contoured in bold lines and the contour interval is 1/s.

are developed beneath the free-surface and above the bottom. Also, the vortices generated between the free-surface and the top of the projecting part are observed in this figure. Fig. 8 shows the influence of bottom in the shedding motion of vortex component O_3. That is, it is clearly observed that the breadth of the wake flow region on the X-Y plane K=5 is narrower than that on the plane K=11. Here X-Y plane number K is same as observed in Fig. 5.

The simulated wave contour maps are shown in Fig. 9. An intensive non-linear waves are developed just behind the shear flow layer of the free-surface. Fig. 10 shows the pressure contour map of each X-Y plane when T=25.0. It is found that the intensive non-linear waves are not dependent upon the pressure distribution of the X-Y planes below the free-surface. This may be presumably due to a locally strong non-linear interaction between the vortices and the free-surface.

Fig. 11 and 12 show the pressure distribution along the model surface at the X-Y sections and a X-Z section, respectively. Although the grid spacing is not sufficiently fine, the pressure distributions on the model surface are not so fluctuated except for the regions of flow separation.

4. Concluding remarks

In the framework of a rectangular coordinate system, a numerical method is developed for the simulation of a three-dimensional viscous flow around a submerged body under the free-surface. In order to investigate the availability of the present method, a flow past a projecting part of sea-bottom is numerically simulated in a shallow water condition. The complicated interaction phenomena of the vortecies which are shedded from the projecting part were demonstrated

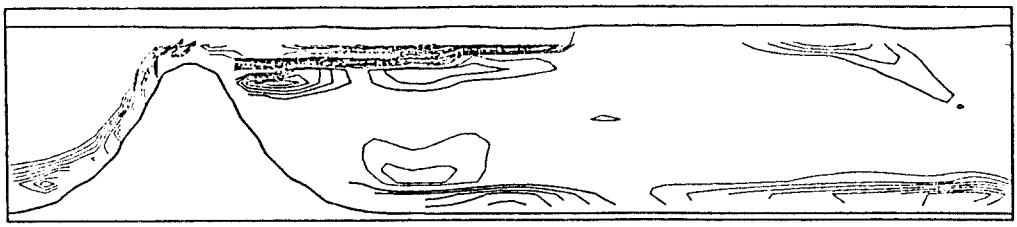

02 Conuour X−Z PL. J=28 NT=2000 T=16.7

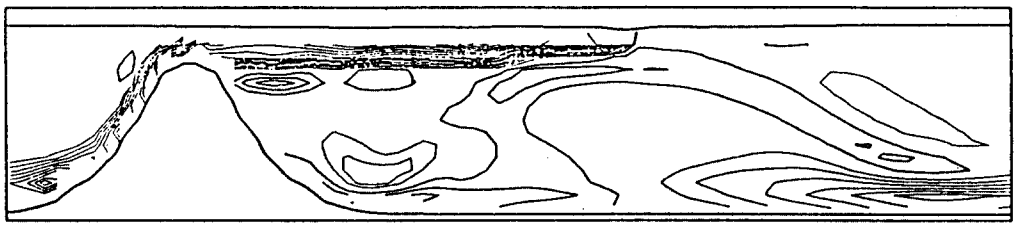

02 Conuour X−Z PL. J=28 NT=2250 T=18.7

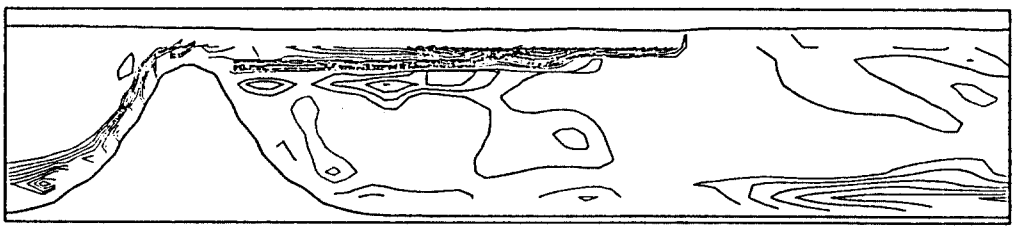

02 Conuour X−Z PL. J=28 NT=2500 T=20.8

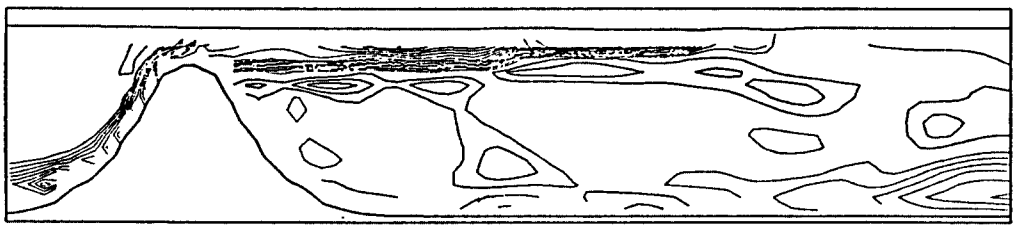

02 Conuour X−Z PL. J=28 NT=2750 T=22.9

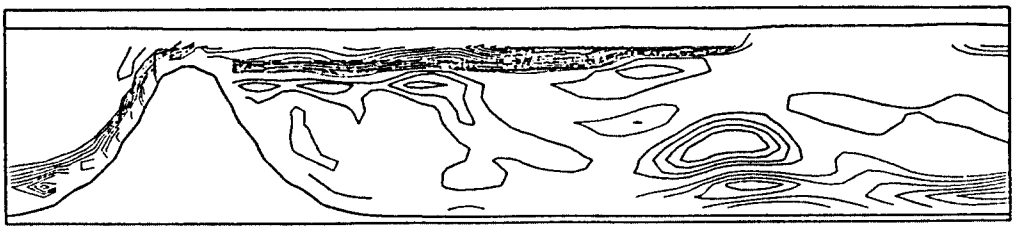

02 Conuour X−Z PL. J=28 NT=3000 T=25.0

Fig. 7 Vorticity contour maps on the X-Z plane J=28. Anticlockwise vorticity is contoured in bold lines and the contour interval is 1/s.

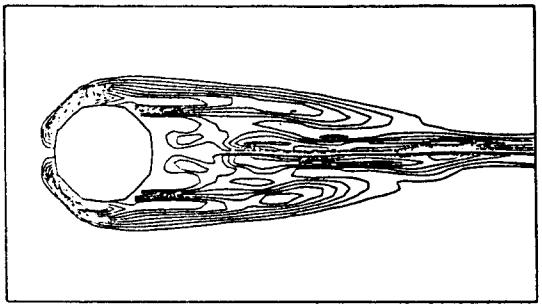

03 Contour X-Y PL. K=5 NT=2250 T=18.7

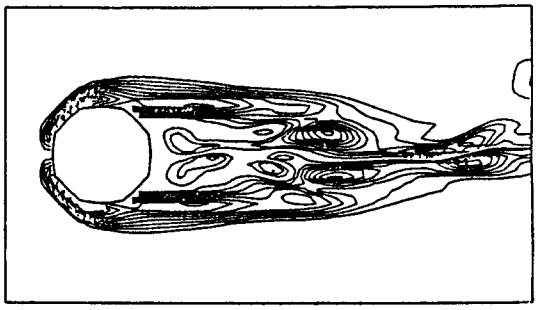

03 Contour X-Y PL. K=5 NT=2750 T=22.9

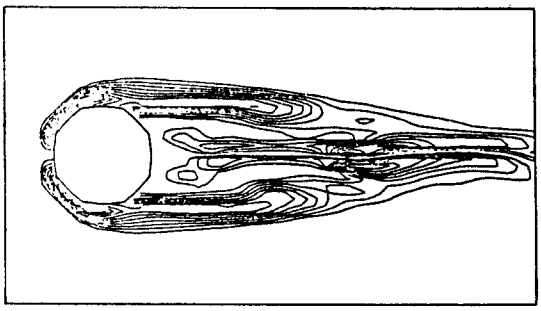

03 Contour X-Y PL. K=5 NT=2500 T=20.8

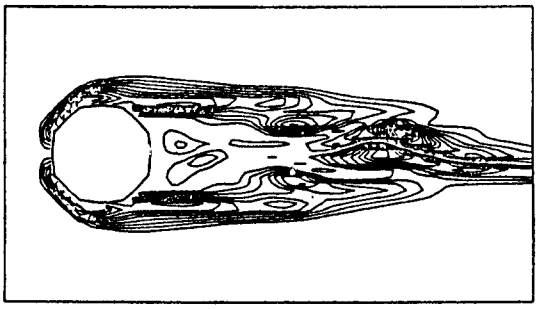

03 Contour X-Y PL. K=5 NT=3000 T=25.0

Fig. 8 Vorticity contour maps on the X-Y plane K=5 and K=11. Anticlockwise vorticity is contoured in bold lines and the contour interval is 1/s.

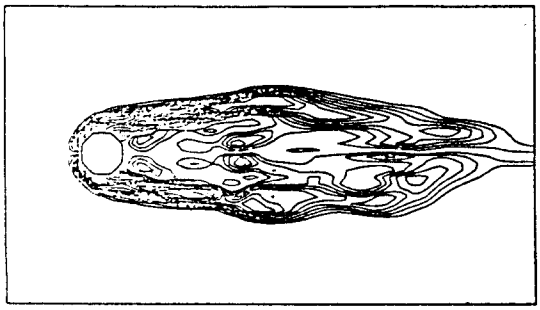

03 Contour X-Z PL. K=11 NT=2250 T=18.7

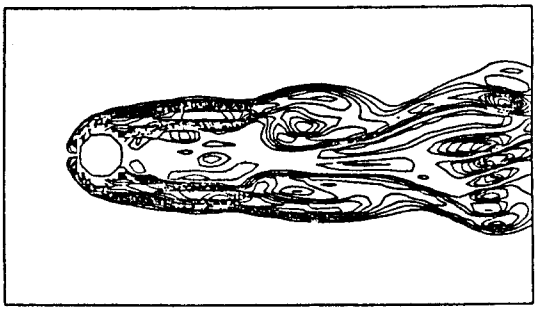

03 Contour X-Z PL. K=11 NT=2750 T=22.9

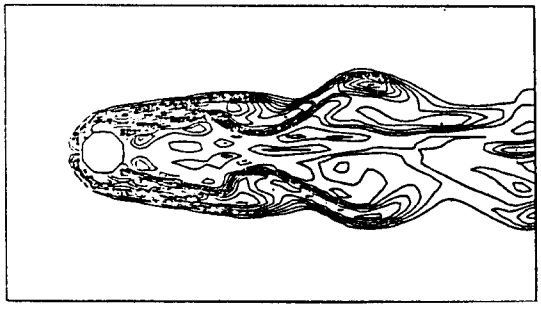

03 Contour X-Z PL. K=11 NT=2500 T=20.8

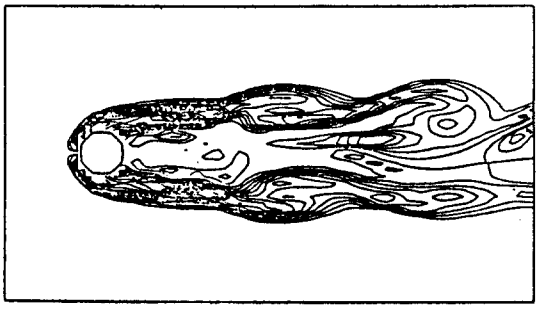

03 Contour X-Z PL. K=11 NT=3000 T=25.0

Fig. 8 (Continued)

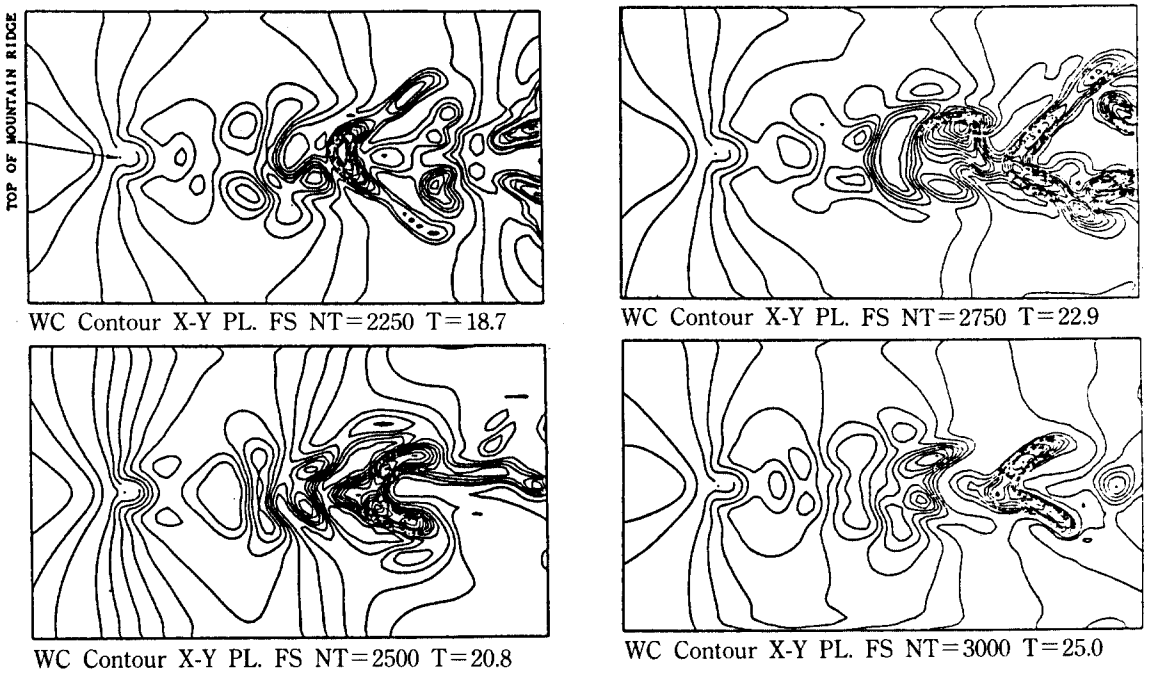

Fig. 9 Wave contour maps above a submerged isolated ridge. Positive wave height is drawn in bold lines and the contour interval is 0.25mm.

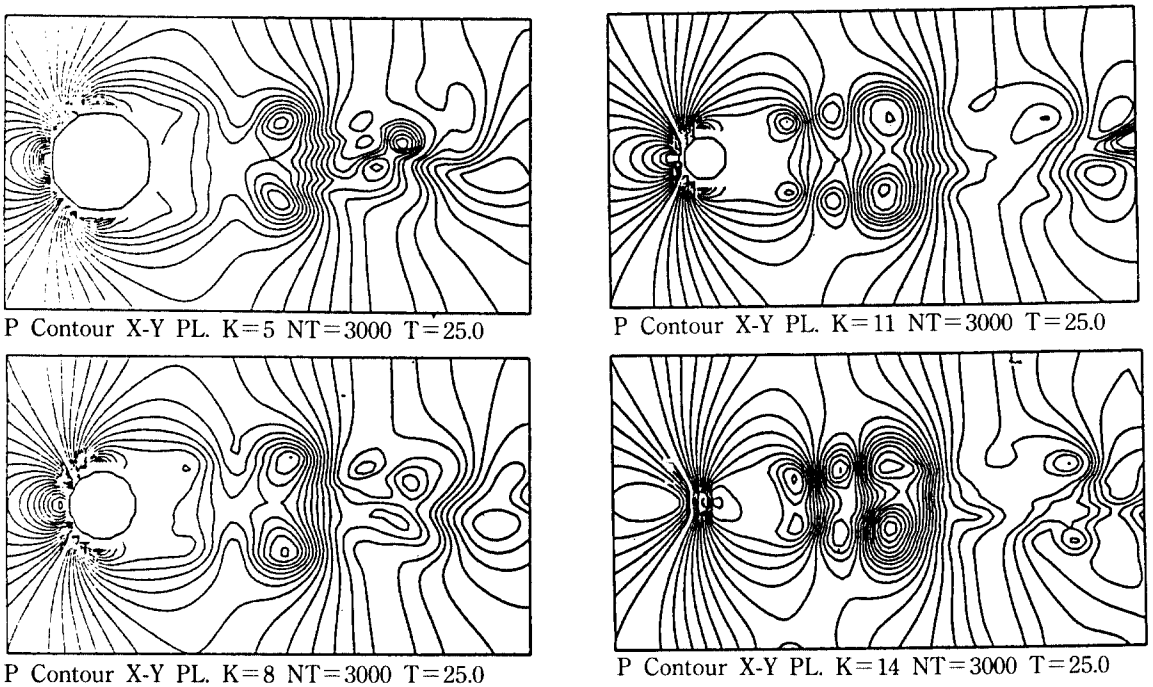

Fig. 10 Pressure contour maps around a submerged isolated ridge at T=25.0. Positive pressure coefficient is drawn in bold lines and the contour interval is 0.05.

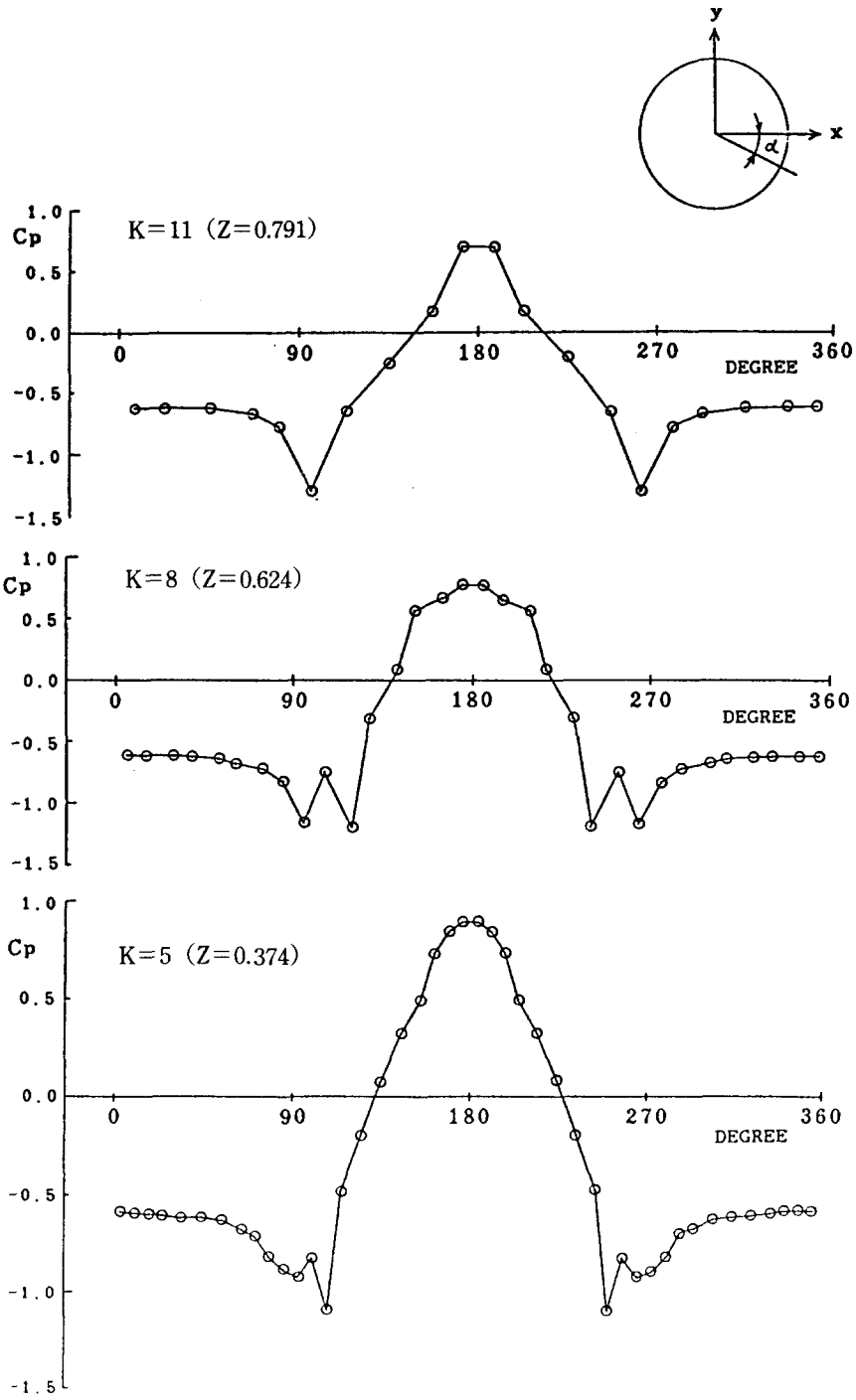

Fig. 11 Pressure distribution on a submerged isolated ridge at the X-Y sections K=5, 8 and 11, T=25.0.

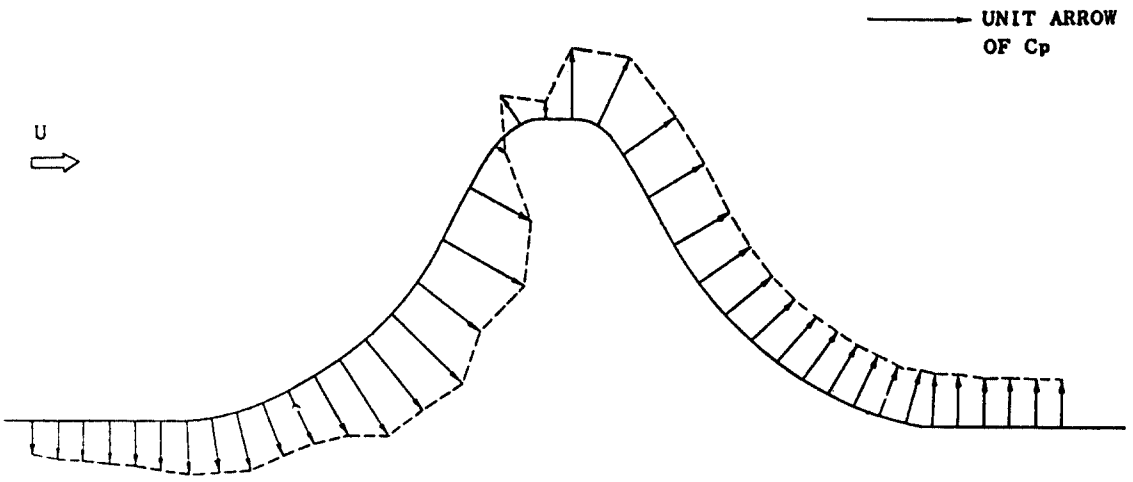

Fig. 12 Pressure distribution on a submerged isolated ridge at the X-Z section Y=0.0, T=25.0.

roughly. The present method is expected to be very useful for the analysis of the complicated three-dimensional viscous flow about an arbitrary object in ocean problems. Although the degree of computational accuracy is not partially sufficient for the resolution of the physical phenomena in the vicinity of the body surface as shown in the surface pressure distributions and vorticity contour maps, it could be improved by the introduction of a multi-grid method in the near future.

Acknowledgements

The computations of this research were executed by a computer HITAC M-680H in the computer center of the University of Tokyo. The CPU time was about 25 hours for the main computation in this paper. The present work is partly supported by the Grant-in-Aid for Cooperative Research of the Ministry of Education, Science and Culture and also by the LINEC research group organized with shipbuilding companies in Japan. The authors are thankful to Professor H. Kajitani for his encouragement and Miss J.-H. Kim for her careful typewriting.

References

1. Y. Yamada and H. Miyata, "A Finite-Difference Method for a Separating Flow Past a Body of Arbitrary Geometry in Rectangular Coordinate Systems", J. Soc. Naval Archit., Jpn, Vo. 167, pp. 17~24, June 1990.
2. Y.-G. Lee and H. Miyata, "A Finite-Difference Simulation Method for 2D Flows about Bodies of Arbitrary Configuration", J. Soc. Naval Archit., Jpn, Vol. 167, pp. 1~8, June 1990.
3. H. Miyata and Y.-G. Lee, "Vortex Motions about a Horizontal Cylinder in Waves", Ocean Eng., Vol. 17, No. 3, pp. 279~305, 1990.
4. Y.-G. Lee, H. Miyata and H. Kajitani, "Some Applications of the TUMMAC Method to 3D Water-wave Problems", J. Soc. naval Archit., Korea, Vol. 25, No. 4, pp. 13~27, Dec. 1988.
5. D. D. Houghton and A. Kasahara, "Nonlinear Shallow Fluid Flow Over an Isolated Ridge", Comm. Pure Appl. Math., Vol. 21, pp. 1~23, 1968.

6. V. R. Lamb and R. E. Britter, "Shallow Flow Over an Isolated Obstacle", J. Fluid Mech., Vol. 147, pp. 291~313, 1984.
7. H. Miyata, C. Matsukawa and H. Kajitani, "A Separating Flow Near the Free Surface", Osaka International Colloquium on Ship Viscous Flow, Japan, 1985.
8. M. J. P. Cullen, "Implicit Finte Difference Methods for Modelling Discontinuous Atmospheric Flows", J. Comput. Phys. 81, pp. 319~348, 1989.
9. Y.-G. Lee., "A Finite Difference Simulation Method for the Viscous Flow with Free Surface by Using Rectangular Coordinate Systems", Doctor thesis, the Univ. of Tokyo, september 1989(in Japanese).
10. R. K. C. Chan and R. L. Street, "A Computer Study of Finite-Amplitude Water Waves", J. Comput. Phys. 6, pp. 68~94, 1970.
11. J. W. Deardorff, "A Numerical Study of Three-Dimensional Turbulent Channel Flow at Large Reynolds Numbers", J. Fluid Mech., Vol. 41, Part 2, pp. 453~480, 1970.